A Mechanistic Dichotomy in Two-Electron Reduction of Dioxygen Catalyzed by *N,N'*-Dimethylated Porphyrin Isomers

Wataru Suzuki, Hiroaki Kotani, Tomoya Ishizuka, and Takahiko Kojima*

Abstract: Selective two-electron reduction of dioxygen (O_2) to hydrogen peroxide (H_2O_2) has been achieved by two saddle-distorted *N,N'*-dimethylated porphyrin isomers, an *N*21,*N'*22-dimethylated porphyrin (***anti*-Me$_2$P**) and an *N*21,*N'*23-dimethylated porphyrin (***syn*-Me$_2$P**) as catalysts and ferrocene derivatives as electron donors in the presence of protic acids in acetonitrile. The higher catalytic performance in an oxygen reduction reaction (ORR) was achieved by ***anti*-Me$_2$P** with higher turnover number (TON = 250 for 30 min) than that by ***syn*-Me$_2$P** (TON = 218 for 60 min). The reactive intermediates in the catalytic ORR were confirmed to be the corresponding isophlorins (***anti*-Me$_2$Iph** or ***syn*-Me$_2$Iph**) by spectroscopic measurements. The rate-determining step in the catalytic ORRs was concluded to be proton-coupled electron-transfer reduction of O_2 with isophlorins based on kinetic analysis. The ORR rate by ***anti*-Me$_2$Iph** was accelerated by external protons, judging from the dependence of the observed initial rates on acid concentrations. In contrast, no acceleration of the ORR rate with ***syn*-Me$_2$Iph** by external protons was observed. The different mechanisms in the O_2 reduction by the two isomers should be derived from that of the arrangement of hydrogen bonding of a O_2 with inner N*H* protons of the isophlorins.

Introduction

Oxygen reduction reaction (ORR) is recognized as one of the most fundamental reactions in biological processes for cellular respiration and chemical technologies such as fuel cells.[1] In addition, hydrogen peroxide (H_2O_2), a two-electron-reduced product of dioxygen (O_2), is widely required for the industrial usage for paper bleaching, a liquid fuel in the component of fuel cells, and an environmentally benign oxidant.[2] H_2O_2 has been industrially supplied through the "anthraquinone process", which is achieved by two-electron ORR. However, there are serious issues to be solved in this process: Rare-metal catalysts have been employed to proceed catalytic hydrogenation of an anthraquinone derivative by a hydrogen gas.[3] Thus, alternative catalysts for efficient and selective H_2O_2 production have been highly demanded without using precious metals.

So far, electrocatalytic,[4] photocatalytic,[5-8] and thermal[9-14] O_2 reduction to afford H_2O_2 have been achieved by redox-active metal complexes having Co[9-12] and Cu[13] centers. Instead of transition metal catalysts, redox-active organic molecules including flavin derivatives,[15] porphyrinoids,[16,17] and carbon-based materials[18] also have been reported as ORR catalysts for selective two-electron reduction of O_2. Compared with metal catalysts, redox-active organic molecules are able to reduce O_2 to H_2O_2 selectively because side-reactions such as disproportionation or decomposition of H_2O_2 by metal catalysts[8e] can be suppressed. In addition, compared with coordinate bonds in metal complexes, the weaker non-covalent interaction of organocatalysts with O_2 would prevent the O–O bond cleavage to form H_2O as a four-electron reduced product of O_2 and other radical species such as hydroxyl (•OH) and hydroperoxyl (•OOH) radicals, showing high selectivity in the formation of H_2O_2. For example, the importance of hydrogen-bonding interaction between N*H* protons of a porphyrinoid and O_2 has been suggested in ORRs catalyzed by metal-free porphyrinoids.[16,17] While the hydrogen bonding also work as a factor to decrease the activation barrier of ORR by trapping the O_2 molecule, the relationship between the ORR reactivity for H_2O_2 production and the strength of hydrogen bonding is still unclear. This should be mainly due to the difficulty of changing the arrangement of hydrogen bonding with O_2 without changing other physical properties such as redox potentials.

In this context, saddle-distorted porphyrins[19] should be a good candidate for the evaluation of ORR reactivity owing to well-known synthetic procedure,[20] redox properties,[21-24] and availability of pyrrolic N*H* protons as hydrogen-bonding sites.[25] Recently, we have synthesized *N,N'*-dimethylated saddle-distorted porphyrin isomers, ***syn*-Me$_2$P** and ***anti*-Me$_2$P** (Scheme 1), having two methyl groups at the different position on inner nitrogen atoms of the porphyrin framework, while the molecular conformation and redox potentials of two isomers were almost the same.[26] Moreover, we established reversible O_2/H_2O_2 conversion by using ***syn*-Me$_2$P** and the corresponding isophlorin derivative (***syn*-Me$_2$Iph**) as a two-electron reduced species, through the two-point hydrogen-bonding interaction between the porphyrinoids and H_2O_2 or O_2.[26] In stark contrast, ***anti*-Me$_2$P** or the corresponding isophlorin derivative (***anti*-Me$_2$Iph**) were

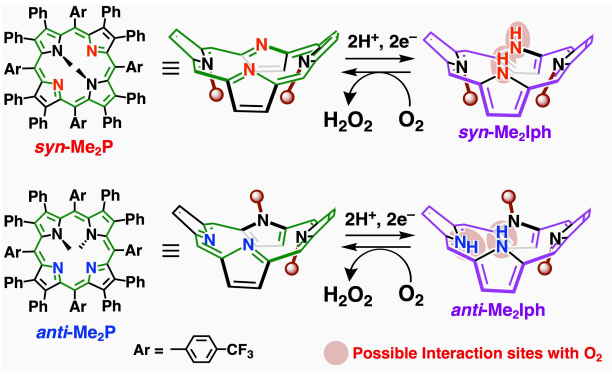

Scheme 1. Overview of formation of *N,N'*-dimethylated isophlorin derivatives for selective two-electron reduction of O_2 to H_2O_2.

Department of Chemistry, Faculty of Pure and Applied Sciences, University of Tsukuba, 1-1-1 Tennoudai, Tsukuba, Ibaraki 305-8571, Japan.
E-mail: kojima@chem.tsukuba.ac.jp.

Electronic Supplementary Information (ESI) available: Crystallographic data of *syn*-$H_2Me_2P^{2+}(CF_3COO^-)_2$ in the CIF format, ^{1}H NMR, UV-vis, and electrochemical data. CCDC-1954353. See DOI: 10.1039/x0xx00000x

revealed to be ineffective for the reversible conversion of O_2/H_2O_2, suggesting just one-point hydrogen-bonding interaction of the porphyrinoids with H_2O_2 or O_2.[26] Based on the observation, we have hypothesized that the structural difference in the porphyrin isomers would contribute to the catalytic performance in ORR. Herein, we report catalytic and selective two-electron reduction of O_2 to H_2O_2 catalyzed by two kinds of *N*,*N*'-dimethylated porphyrins (***syn*-Me$_2$P** or ***anti*-Me$_2$P**) as catalysts to gain mechanistic insights into ORRs and the controlling factors of the reactivity of the porphyrins as catalysts in ORRs (Scheme 1).

Results and Discussion

Catalytic Reduction of O_2 to H_2O_2 with Me_8Fc as a Reductant using *syn*-Me$_2$P or *anti*-Me$_2$P as a Catalyst

By using ***syn*-Me$_2$P** or ***anti*-Me$_2$P** as a catalyst, we developed catalytic ORR systems to afford H_2O_2 selectively in acetonitrile (CH_3CN) (Scheme 2). Octamethylferrocene (Me_8Fc; E_{ox} = –0.44 V *vs.* Fc/Fc^+ in CH_3CN)[16] and trifluoroacetic acid (TFA) were selected as an electron donor and a proton source, respectively. Note that no H_2O_2 was formed without the catalysts

$$O_2 + 2H^+ + 2Me_8Fc \xrightarrow{\text{cat.}} H_2O_2 + 2Me_8Fc^+$$

cat. = *syn*-Me$_2$P or *anti*-Me$_2$P

Scheme 2. Catalytic O_2 reduction to afford H_2O_2 with Me_8Fc by *N*,*N*'-dimethylated porphyrins in CH_3CN.

Table 1. Summary of reaction conditions, TONs and yields of H_2O_2 production in catalytic reduction of O_2 catalyzed by ***syn*-Me$_2$P** or ***anti*-Me$_2$P**.

Entry	[cat.] / μM	Solv. (v/v)	TON	Yield
1	0	CH_3CN	-	0%
2	10 (***syn*-Me$_2$P**)	CH_3CN	32	64%
3	10 (***anti*-Me$_2$P**)	CH_3CN	50	100%
4	10 (***syn*-Me$_2$P**)	CH_3CN/H_2O = 99/1	45	90%
5	2 (***syn*-Me$_2$P**)	CH_3CN/H_2O = 90/10	218	87%
6	2 (***anti*-Me$_2$P**)	CH_3CN/H_2O = 90/10	250	100%
7	0	CH_3CN/H_2O = 90/10	-	6%

Catalytic conditions: [TFA] = 3 mM, [Me_8Fc] = 1 mM, under O_2, at room temperature for 30 min. [a] For 60 min. TON = [H_2O_2]/ [cat.]. Yield (%) = (100 × [H_2O_2]) / (2 × [Me_8Fc]). [H_2O_2] was determined by iodometry.

(Table 1, Entry 1). The amounts of H_2O_2 formed in the catalytic reactions were quantified by iodometry upon addition of excess amounts of potassium iodide (KI) to diluted reaction mixtures after the catalytic reactions.[9b,27] As shown in Table 1, both ***syn*-Me$_2$P** and ***anti*-Me$_2$P** acted as catalysts for two-electron-reduction of O_2 to form H_2O_2 in CH_3CN. While the turnover number (TON) of the H_2O_2 production by ***syn*-Me$_2$P** was determined to be 32 with 64% yield based on the amount of Me_8Fc used (Entry 2), TON for ***anti*-Me$_2$P** was reached to 50 in 100% yield (Entry 3). Upon addition of 1% H_2O in CH_3CN, TON of catalytic H_2O_2 production with use of ***syn*-Me$_2$P** was improved to be 45 and the yield of H_2O_2 was 90% based on the amount of Me_8Fc used (Entry 4). When the water contents increased up to 10% in CH_3CN, maximum TONs were reached to 218 (87% yield) for 1 h for ***syn*-Me$_2$P** (Entry 5) and 250 (100% yield) for 30 min for ***anti*-Me$_2$P** (Entry 6), although the yield of H_2O_2 was negligible in the absence of the catalysts (Entry 7). These TONs were higher than those of previously reported metal-free O_2 reduction catalysts.[16,17]

Characterization of Reduced Species of *syn*-Me$_2$P and *anti*-Me$_2$P in the Presence of Protons

To reveal the origin of the difference in the reactivity between ***syn*-Me$_2$P** and ***anti*-Me$_2$P** in the catalytic ORR, electrochemical measurements of ***syn*-Me$_2$P** and ***anti*-Me$_2$P** were performed for the comparison of their redox potentials ($E_{1/2}$) in deaerated CH_3CN solutions in the presence of TFA and [(*n*-butyl)$_4$N](PF_6) ($TBAPF_6$) as an electrolyte (Figure S1). In the presence of excess amount of acids, saddle-distorted porphyrins such as dodecaphenylporphyrin (**H$_2$DPP**) were easily protonated to form diprotonated ones such as **H$_4$DPP^{2+}**.[19b] Since ***syn*-Me$_2$P** and ***anti*-Me$_2$P** also were confirmed to show highly saddle-distorted conformations,[26] they were protonated by TFA to form the corresponding diprotonated species (***syn*-H$_2$Me$_2$P^{2+}** and ***anti*-H$_2$Me$_2$P^{2+}**), as confirmed by UV-vis spectroscopic and X-ray crystallographic analysis (Figure S2 and S3). Thus, we observed redox waves of ***syn*-H$_2$Me$_2$P^{2+}** and ***anti*-H$_2$Me$_2$P^{2+}** under the electrochemical conditions, as described below. Electrochemical data of ***syn*-H$_2$Me$_2$P^{2+}** showed one reversible two-electron reduction at –0.38 V *vs.* Fc/Fc^+ (Figure S1a) due to the disproportionation of one-electron reduced species as observed for **H$_4$DPP^{2+}**.[28] On the other hand, two reversible redox waves were observed at –0.33 V and –0.44 V *vs.* Fc/Fc^+ in the case of ***anti*-H$_2$Me$_2$P^{2+}** (Figure S1b), suggesting the stepwise one-electron reduction of ***anti*-H$_2$Me$_2$P^{2+}** to form two-electron reduced species. The reason why the stepwise redox processes of ***anti*-H$_2$Me$_2$P^{2+}** is probably the slow disproportionation of one-electron reduced species of ***anti*-H$_2$Me$_2$P^{2+}** (***anti*-H$_2$Me$_2$P$^{\bullet+}$**). The redox potentials ($E_{1/2}$) determined in CH_3CN containing excess TFA were slightly higher than those in DMF (–0.43 V *vs.* Fc/Fc^+ for ***syn*-H$_2$Me$_2$P^{2+}** and –0.47 V *vs.* Fc/Fc^+ for ***anti*-H$_2$Me$_2$P^{2+}**).[22] Thus, such small difference of redox potentials between ***syn*-H$_2$Me$_2$P^{2+}** and ***anti*-H$_2$Me$_2$P^{2+}** should not affect the difference of reactivity in catalytic ORR between ***syn*-Me$_2$P** and ***anti*-Me$_2$P** (Table 1).

Next, to characterize two-electron-reduced species of ***syn*-Me$_2$P** or ***anti*-Me$_2$P** in the presence of excess TFA (pK_a = 12.6 in

CH_3CN)[29,30] under Ar, chemical reduction by Me_8Fc was scrutinized by UV-vis and NMR measurements at 298 K (Schemes 3 and 4). Upon addition of Me_8Fc (1.0 mM) to a deaerated CH_3CN solution containing ***syn*-Me$_2$P** (0.010 mM) with TFA (3.0 mM), absorption bands at 503 and 730 nm derived from ***syn*-H$_2$Me$_2$P^{2+}**, which was formed by diprotonation of ***syn*-Me$_2$P** with TFA (Figure S2), disappeared with simultaneous appearance of an absorption band at 450 nm as shown in Figure 1. The observed UV-vis spectral change indicated the formation of an isophlorin derivative (***syn*-Me$_2$Iph**) because the spectral change was comparable with that observed in the reaction of ***syn*-Me$_2$P** with an aqueous solution of $Na_2S_2O_4$ in deaerated DMF.[22] In addition, a ^{19}F NMR spectrum of ***syn*-Me$_2$P** in the presence of TFA and Me_8Fc in CD_3CN showed a single peak at –63.4 ppm, reflecting the C_{2v} symmetric structure of ***syn*-Me$_2$Iph** (Figure S4).

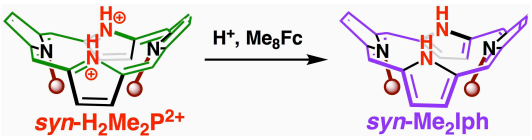

Scheme 3. Chemical reduction of ***syn*-H$_2$Me$_2$P^{2+}** to form the corresponding isophlorin derivative (***syn*-Me$_2$Iph**) in the presence of an acid.

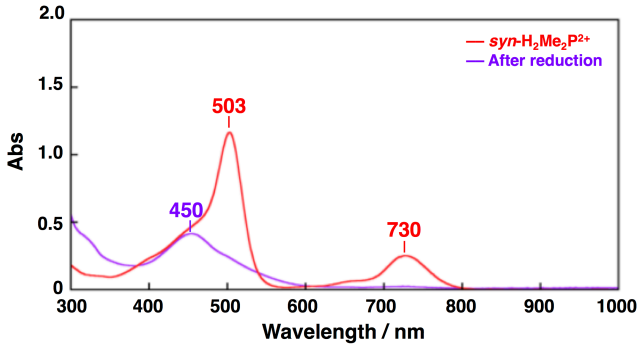

Figure 1. UV-vis spectral change of ***syn*-Me$_2$P** (0.010 mM) before (red) and after (purple) the reduction with Me_8Fc (1.0 mM) in the presence of TFA (3.0 mM) in deaerated CH_3CN at 298 K.

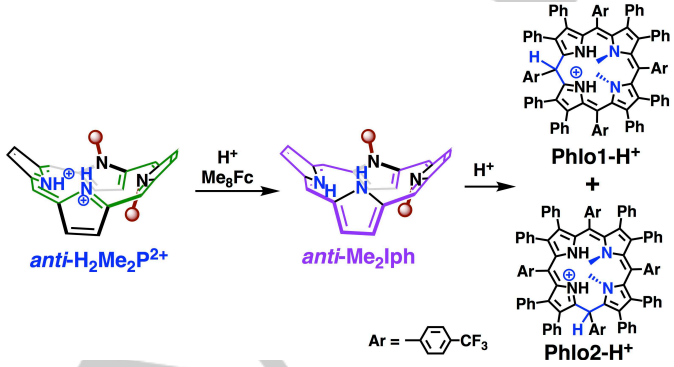

Scheme 4. Chemical reduction of ***anti*-Me$_2$P** in the presence of an acid to form protonated phlorins.

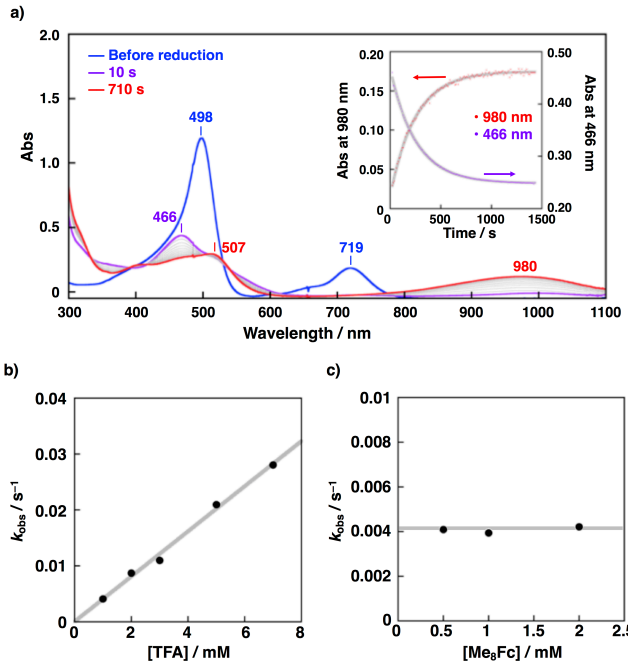

Figure 2. a) UV-vis spectral changes of ***anti*-Me$_2$P** (0.010 mM) in the course of the reduction with Me_8Fc (0.50 mM) in the presence of TFA (1.0 mM) in deaerated CH_3CN at 298 K. b) Time-course of absorbance at 980 nm with curve fitting. c) Dependence of k_{obs} on [TFA] in the presence of Me_8Fc (0.50 mM). d) Dependence of k_{obs} on [Me_8Fc] in the presence of TFA (1.0 mM).

Thus, even in the presence of excess TFA, ***syn*-Me$_2$P** was reduced to form ***syn*-Me$_2$Iph** as a two-electron-reduced product selectively without further transformation or isomerization.

In contrast to the case of ***syn*-Me$_2$P**, chemical reduction of ***anti*-Me$_2$P** by addition of Me_8Fc in CH_3CN containing excess TFA afforded initially the corresponding isophlorin derivative (***anti*-Me$_2$Iph**) through the two-electron reduction of ***anti*-H$_2$Me$_2$P^{2+}**; however, ***anti*-Me$_2$Iph** underwent subsequent isomerization to a protonated phlorin (**Phlo-H$^+$**)[23] as shown in Scheme 4. UV-vis spectrum of ***anti*-Me$_2$Iph** showing the absorption maxima at 466 nm changed to that with absorption bands at 507 nm and around 980 nm derived from **Phlo-H$^+$** (Figure 2a).[23,31] The pseudo-first-order rate constant (k_{obs}) of the protonation-induced isomerization from ***anti*-Me$_2$Iph** to **Phlo-H$^+$** was determined at 298 K to be (4.09 ± 0.02) × 10^{-3} s^{-1} in the presence of TFA (1.0 mM) and Me_8Fc (0.50 mM) on the basis of the time course of absorbance at 980 nm. The rate constant was consistent with that of absorbance at 466 nm (k_{obs} = (3.94 ± 0.02) × 10^{-3} s^{-1}, Figure 2a inset). The k_{obs} values showed linear dependence on the concentration of TFA (Figure. 2b), while no dependence on that of Me_8Fc was observed (Figure 2c). Thus, the rate of the protonation-induced isomerization of ***anti*-Me$_2$Iph** to afford **Phlo-H$^+$** is given by Equation (1):

$$d[\textbf{Phlo-H}^+]/dt = k_{obs}[\textbf{\textit{anti}-Me}_2\textbf{Iph}] = k[\text{TFA}][\textbf{\textit{anti}-Me}_2\textbf{Iph}] \quad (1)$$

On the basis of Equation (1), the second-order rate constant (k) was determined to be (4.0 ± 0.2) M^{-1} s^{-1} from the slope in Figure 2b. When dichloroacetic acid (DCA, pK_a = 15.9 in CH_3CN)[29,30] was used as acids instead of TFA, the second-order rate constant (k) decreased to (1.6 ± 0.4) M^{-1} s^{-1} due to the lower acidity of DCA than that of TFA (Figure S5). This result indicates that the isomerization rates of ***anti*-Me$_2$Iph** depends on not only the pK_a values of acids used but also the concentration of acids as shown in Figure 2b and Figure S5.

Then, we also performed ^{1}H and ^{19}F NMR measurements of **PhIo-H$^+$** in CD_3CN. A ^{1}H NMR spectrum of **PhIo-H$^+$** showed two sets of ^{1}H NMR signals derived from non-equivalent *N*-Me groups at 4.20, 3.82 ppm and 4.52, 4.83 ppm with the intensity ratio of 2:1, accompanied by the observation of singlet signals due to the methine proton on a *meso*-carbon atom at 6.27 ppm and 6.50 ppm with the same integration ratio (Figure S6). In the ^{19}F NMR spectrum, two sets of four non-equivalent signals derived from the trifluoromethyl (CF_3) groups were also observed with the 2:1 integration ratio as depicted in Figure S7, in consistent with the result of ^{1}H NMR measurement. The ^{1}H and ^{19}F NMR spectra reflected the low symmetrical structure of **PhIo-H$^+$**, which should have one imine nitrogen atom and one sp^3 *meso*-carbon atom in the porphyrinoid core.[23] Because the *meso*-carbon atoms of a protonated phlorin bear non-equivalent nature, there are several isomers of **PhIo-H$^+$** depending on the position of an sp^3 *meso*-carbon atom. To compare the thermodynamic stability among structural isomers of the protonated phlorins, DFT calculations on possible three structural isomers (**PhIo(n)-H$^+$**, n = 1-3) were conducted at the B3LYP/6-31G** level of theory. As shown in Figure S8, **PhIo1-H$^+$** having an sp^3 *meso*-carbon atom between two non-methylated NH pyrrole moieties was the most stable among the three isomers, while **PhIo3-H$^+$** having an sp^3 *meso*-carbon atom between two N-Me pyrrole moieties was the most unstable. Then, **PhIo2-H$^+$** having an sp^3 *meso*-carbon atom between one NH pyrrole moieties and N-Me pyrrole moieties was relatively unstable in comparison with **PhIo1-H$^+$** by 4.2 kcal mol^{-1}. Considering that two kinds of methine protons were observed in ^{1}H NMR measurements of the reduced species (Figure S6), **PhIo1-H$^+$** and **PhIo2-H$^+$** should be formed in the 2:1 ratio by chemical reduction of ***anti*-Me$_2$P** in the presence of external protons (Scheme 4). Hereafter "**PhIo-H$^+$**" dictates a mixture of **PhIo1-H$^+$** and **PhIo2-H$^+$**.

Revealing the Reaction Mechanisms in ORR Catalyzed by Dimethylated Porphyrins

To gain mechanistic insights into the catalytic ORR catalyzed by ***syn*-Me$_2$P** and ***anti*-Me$_2$P**, kinetic analyses on ORR were conducted under the catalytic conditions. Thus, for revealing reaction mechanisms of the catalytic H_2O_2 production, decamethylferrocene ($Me_{10}Fc$, E_{ox} = –0.50 V *vs.* Fc/Fc^+ in CH_3CN)[16] was employed as an electron donor to reduce ***syn*-H$_2$Me$_2$P^{2+}** and ***anti*-H$_2$Me$_2$P^{2+}** in the presence of excess TFA. At first, catalytic ORR by ***syn*-Me$_2$P** (0.010 mM) was conducted in CH_3CN containing TFA (1.0 mM) and $Me_{10}Fc$ (0.10 mM) in air-saturated CH_3CN ($[O_2]$ = 2.6 mM, Figure 3).[14b] As shown in Figure 3a, UV-vis spectral change corresponding to the formation of a decamethylferrocenium ion ($Me_{10}Fc^+$) showing the absorption around 800 nm was observed in the course of the catalytic reaction,[16] whereas the absorption band at 450 nm owing to ***syn*-Me$_2$Iph** was maintained after adding $Me_{10}Fc$ as an electron donor (t = 0 s). In addition, the formation rate of $Me_{10}Fc^+$ obeyed zero-order kinetics (Figure 3a, inset). After the consumption of $Me_{10}Fc$, ***syn*-Me$_2$P** was recovered as the diprotonated species (***syn*-H$_2$Me$_2$P^{2+}**) owing to the protonation by excess amount of remained TFA (Figure S9). It should be noted that no decomposition of ***syn*-Me$_2$P** was observed after the catalytic reaction, judging from the comparison of the UV-vis spectra before and after the catalytic reactions (Figure S9). Then, dependence of the zero-order rate (v, mM s^{-1}) of formation of $Me_{10}Fc^+$ on $[Me_{10}Fc]$, $[O_2]$, [***syn*-Me$_2$P**], and [TFA] were investigated by changing the concentration of each component. First-order dependence of v on $[O_2]$ and [***syn*-Me$_2$P**] was observed, while no dependence of v on $[Me_{10}Fc]$ and [TFA] was observed (Figure 3b-e). These results indicate the reaction between ***syn*-Me$_2$Iph** and O_2 is the rate-determining step in the

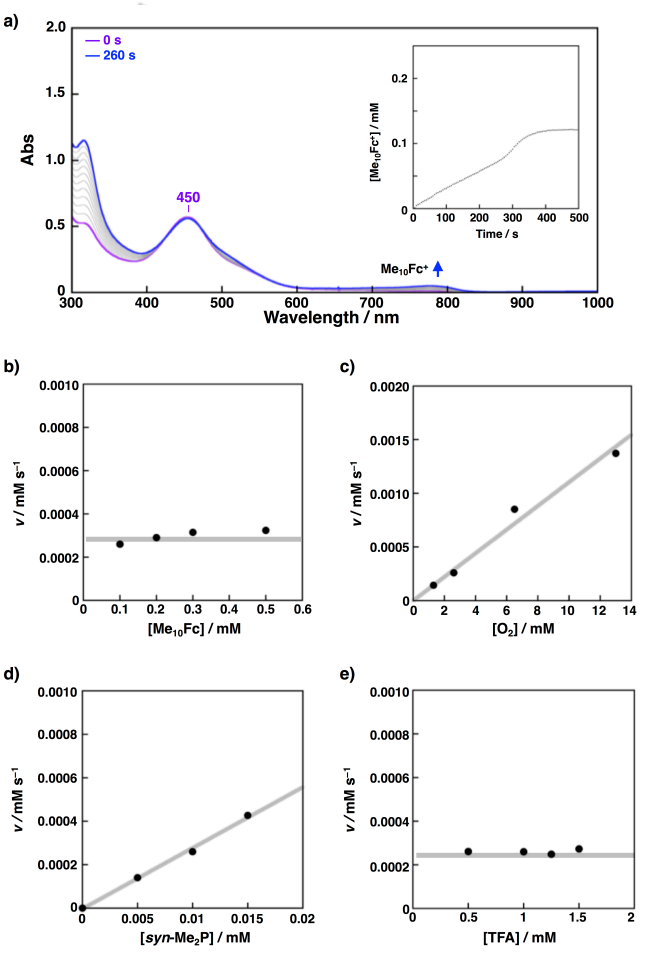

Figure 3. a) UV-vis spectral change in the course of catalytic O_2 reduction catalyzed by ***syn*-Me$_2$P** (0.010 mM) in air-saturated CH_3CN. [TFA] =1.0 mM, $[Me_{10}Fc]$ = 0.10 mM. Inset: Time profile of $[Me_{10}Fc^+]$. b) $[Me_{10}Fc]$ dependence of v. c) $[O_2]$ dependence of v. d) [***syn*-Me$_2$P**] dependence of v. (e) [TFA] dependence of v.

catalytic ORR cycle. Interestingly, no dependence of *v* on acid concentrations was observed (Figure 3e) in spite of the fact that two protons should be needed to form H_2O_2 from O_2. Furthermore, the averaged *v* value ($v = 2.5 \times 10^{-4}$ mM s^{-1}) in the presence of TFA was almost the same as that in the presence of DCA. (Figure 3e, 4, and S10). These kinetic analyses indicate that ***syn*-Me$_2$Iph** reacts with O_2 without acceleration by external protons in the reaction of ***syn*-Me$_2$Iph** with O_2. Therefore, it is considered that ***syn*-Me$_2$Iph** can form a two-point hydrogen bonding with O_2 and reduce O_2 to produce H_2O_2 through proton-coupled electron transfer (PCET) from ***syn*-Me$_2$Iph** to O_2 (Scheme 5a).[26]

In the case of catalytic ORR by ***anti*-Me$_2$P**, ***anti*-Me$_2$Iph** or **Phlo-H$^+$** can be possible reactive intermediates for catalytic H_2O_2 production as described above. Thus, the reactivity of ***anti*-Me$_2$Iph** and **Phlo-H$^+$** toward O_2 was qualitatively compared by changing the reaction conditions in CH_3CN (Figure S11 and S12). When slightly excess amounts of $Me_{10}Fc$ was used for the reduction of ***anti*-Me$_2$P** under O_2 in the presence of excess amounts of TFA, ***anti*-Me$_2$Iph** was formed and smoothly reacted with O_2 to form ***anti*-H$_2$Me$_2$P^{2+}** within 10 seconds, while the formation of **Phlo-H$^+$** was hardly observed under the conditions (Figure S11). On the other hand, the reaction of **Phlo-H$^+$** with O_2 was significantly slow when O_2 was introduced after the formation of **Phlo-H$^+$**, which was generated by reduction of ***anti*-Me$_2$P** with $Me_{10}Fc$ in the presence of excess amounts of TFA under Ar (Figure S12). Therefore, the reactivity of ***anti*-Me$_2$Iph** with O_2 is much higher than that of **Phlo-H$^+$** in the catalytic reduction of O_2, suggesting the reaction intermediate in ORR catalyzed by ***anti*-Me$_2$P** should be ***anti*-Me$_2$Iph**, not **Phlo-H$^+$**. The pseudo-first-order rate constant of the reaction of ***anti*-Me$_2$Iph** with O_2 in the presence of TFA (1.0 mM) was determined to be 0.5 s^{-1} (Figure S11), which was much larger than that of the proton-assisted isomerization of ***anti*-Me$_2$Iph** to form **Phlo-H$^+$** (0.005 s^{-1}) in the presence of TFA (1.0 mM) as shown in Figure 2. Thus, in the presence of O_2, ORR by ***anti*-Me$_2$Iph** should proceed much faster than the isomerization under the catalytic conditions without suffering from the isomerization.

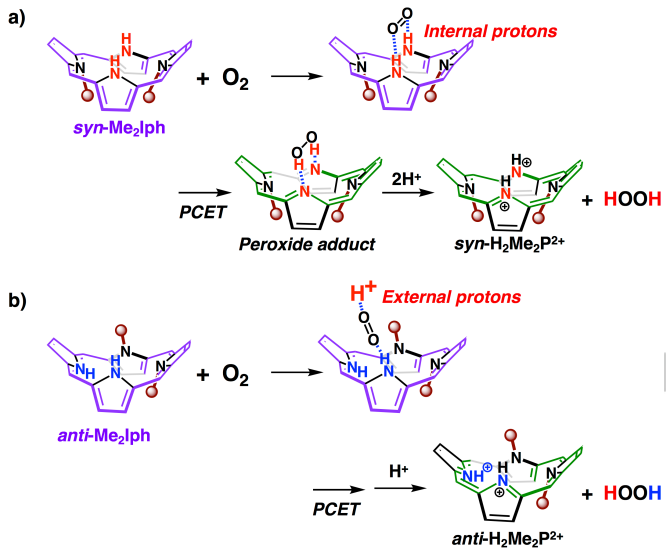

Scheme 5. Comparison of reaction mechanisms in two-electron-reduction of O_2 by a) ***syn*-Me$_2$Iph** or b) ***anti*-Me$_2$Iph**.

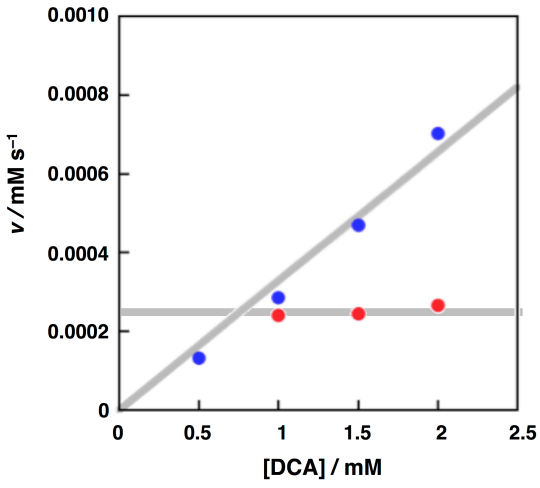

Figure 4. Plots of zero-order rate (*v*) vs [DCA] in the catalytic H_2O_2 production by ***syn*-Me$_2$P** (red circle) and ***anti*-Me$_2$P** (blue circle).

Next, kinetic analysis in the catalytic reduction of O_2 by ***anti*-Me$_2$P** was examined. To suppress the transformation of ***anti*-Me$_2$Iph** to **Phlo-H$^+$** by external protons, DCA was selected as a proton source (Figure S5). In the case of the reduction of O_2 catalyzed by ***anti*-Me$_2$P** in the presence of excess DCA, formation of ***anti*-Me$_2$Iph** was observed in UV-vis measurements during the catalytic reaction in CH_3CN containing DCA (1.0 mM) and $Me_{10}Fc$ (0.10 mM), indicating ***anti*-Me$_2$Iph** should be a reactive intermediate (Figure S13). Due to the partial formation of **Phlo-H$^+$**, the yield of ***anti*-Me$_2$P** after the catalytic reaction was slightly decreased on the basis of the comparison of absorbance at 494 nm before and after the catalytic reaction (Figure S14). The formation rate of $Me_{10}Fc^+$ obeyed zero-order kinetics (Figure S13, inset). Furthermore, linear correlation was observed between *v* and [O_2] as shown in Figure S15. Therefore, the rate-determining step in the catalytic cycle was also concluded to be the reaction of ***anti*-Me$_2$Iph** with O_2. In contrast to the case of ***syn*-Me$_2$P**, first-order dependence of *v* of formation of $Me_{10}Fc^+$ on [DCA] was observed when using ***anti*-Me$_2$P** as a catalyst (Figure. 4, blue circle). In addition, *v* of the ORR catalyzed by ***anti*-Me$_2$P** was higher than that by ***syn*-Me$_2$P** in the presence of more than 1 mM of DCA as shown in Figure 4. The first-order dependence of the zero-order rate constant on [DCA] indicates that an external proton is involved in the rate-determining step in the catalytic cycle in use of ***anti*-Me$_2$P** as the catalyst.[32] Since N*H* protons of ***anti*-Me$_2$Iph** should be oriented to different directions relative to the mean plane of the saddle-distorted macrocycle, only one-point hydrogen bonding should be available between ***anti*-Me$_2$Iph** and O_2 in the course of ORR (Scheme 5b). This assumption was supported by DFT calculations on the O_2 adduct of ***anti*-Me$_2$Iph** (***anti*-Me$_2$Iph-O$_2$**, Figure S16) to indicate the formation of single-point hydrogen bonding between an oxygen atom of O_2 and a proton on one of the pyrrole nitrogen atoms. Thus, the distal

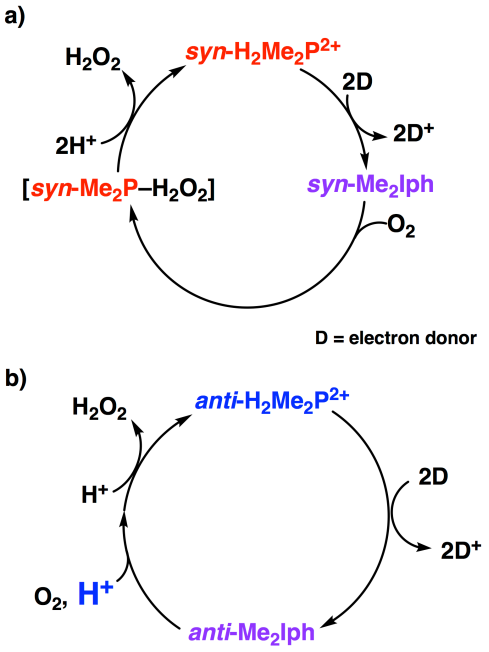

Figure 5. Proposed catalytic cycles of two-electron reduction of O_2 to H_2O_2 catalyzed by a) ***syn*-Me$_2$P** and b) ***anti*-Me$_2$P**. D = Electron donor.

oxygen atom of O_2 is able to accept an external proton from an acid such as DCA, accelerating the proton-coupled reduction of O_2 by ***anti*-Me$_2$Iph**. Therefore, higher catalytic reactivity of ***anti*-Me$_2$P** than that of ***syn*-Me$_2$P** could be observed under catalytic conditions where excess proton source existed (Scheme 5). Proposed catalytic cycles of two-electron reduction of O_2 to H_2O_2 catalyzed by ***syn*-Me$_2$P** and ***anti*-Me$_2$P** are summarized in Figure 5. In the case of ***syn*-Me$_2$P**, as depicted in Figure 5a, thermal ET from an electron donor such as Me_8Fc to ***syn*-H$_2$Me$_2$P^{2+}** affords the two-electron-reduced species, ***syn*-Me$_2$Iph**, as the responsible intermediate for the ORR in the presence of a proton source such as TFA and DCA. The reduced species, ***syn*-Me$_2$Iph**, interacts directly with O_2 through two-point hydrogen bonding and reduces O_2 to form H_2O_2 without the aid of external protons.[26] After releasing H_2O_2, the ***syn*-Me$_2$P** is recovered and diprotonated by the proton source to regenerate ***syn*-H$_2$Me$_2$P^{2+}**. On the other hand, in the case of ***anti*-Me$_2$P** (Figure. 5b), after forming ***anti*-Me$_2$Iph** *via* thermal ET from an electron donor to ***anti*-H$_2$Me$_2$P^{2+}**, the two-electron reduced species interacts with O_2 through single-point hydrogen bonding. The captured O_2 molecule picks up one external proton from an external proton source such as TFA and DCA to be reduced by ***anti*-Me$_2$Iph**, affording H_2O_2. After releasing H_2O_2, the resultant ***anti*-Me$_2$P** is diprotonated by the proton source to recover ***anti*-H$_2$Me$_2$P^{2+}**.

Conclusions

In summary, we have developed catalytic systems for selective two-electron reduction of O_2 to afford H_2O_2 by *N*,*N*'-dimethylated saddle-distorted porphyrin isomers (***syn*-Me$_2$P** and ***anti*-Me$_2$P**) as metal-free organocatalysts. The high selectivity and the highest TON for H_2O_2 production among homogeneous metal-free catalysts were achieved by using these two structural isomers and ***anti*-Me$_2$P** showed higher reactivity than ***syn*-Me$_2$P**. The reaction intermediates in the ORR catalyzed by ***syn*-Me$_2$P** and ***anti*-Me$_2$P** were the corresponding isophlorin derivatives (***syn*-Me$_2$Iph** and ***anti*-Me$_2$Iph**, respectively), which are two-electron reduced porphyrins having two inner N*H* protons at the macrocycle core. On the other hand, protonated phlorins (**Phlo-H$^+$**), formed through the reaction of ***anti*-Me$_2$Iph** with external protons, showed much less reactivity toward O_2 than that of isophlorin derivatives. The ORR mechanisms are drastically changed by the positions of N*H* protons in ***syn*-Me$_2$Iph** and ***anti*-Me$_2$Iph**: Single-point hydrogen bonding between ***anti*-Me$_2$Iph** and O_2 play an important role to promote O_2 reduction by virtue of further strong interactions with external protons. Thus, the arrangement and hydrogen-bonding abilities of N*H* protons of reduced porphyrinoids with O_2 should be crucial to control their reactivity in metal-free ORR catalysis.

Acknowledgements

This work was supported by a Grant-in-Aid (17H03027) from the Japan Society of Promotion of Science (JSPS, MEXT) of Japan and the Cooperative Research Program of "Network Joint Research Center for Materials and Devices". Financial support through CREST (JST) is also appreciated (JPMJCR16P1). W.S. appreciates a support from JSPS Research Fellowship for Young Scientists (18J12184).

Keywords: Oxygen reduction reaction (ORR) • Non-planar porphyrin • Isophlorin • Hydrogen bonding • Organocatalysts

[1] a) J. J. Warren, T. A. Tronic, J. M. Mayer, *Chem. Rev.* **2010**, *110*, 6961-7001; b) M. L. Pegis, C. F. Wise, D. J. Martin, J. M. Mayer, *Chem. Rev.* **2018**, *118*, 2340-2391; c) C. W. Machan, *ACS Catal.* **2020**, *10*, 2640-2655.

[2] a) S. Fukuzumi, *Joule* **2017**, *1*, 689-738; b) S. Fukuzumi, Y.-M. Lee, W. Nam, *Chem. Eur. J.* **2018**, *24*, 5016-5031; c) S. Fukuzumi, Y.-M. Lee, W. Nam, *ChemCatChem* **2018**, *10*, 9-28.

[3] a) J. M. Campos-Martin, G. Blanco-Brieva, J. L. G. Fierro, *Angew. Chem. Int. Ed.* **2006**, *45*, 6962-6984; b) T. Nishimi, T. Kamachi, T. Kato, K. Yoshizawa, *Eur. J. Org. Chem.* **2011**, 4113-4120; c) Y. Guo, C. Dai, Z. Lei, *Chem. Eng. Sci.* **2017**, *172*, 370-384.

[4] a) S. Yang, J. Kim, Y. J. Tak, A. Soon, H. Lee, *Angew. Chem. Int. Ed.* **2016**, *55*, 2058-2062; b) S. Yang, A. Verdaguer-Casadevall, L. Arnarson, L. Silvioli, V. Čolić, R. Frydendal, J. Rossmeisl, I. Chorkendorff, I. E. L. Stephens, *ACS Catal.* **2018**, *8*, 4064-4081.

[5] a) S. J. Freakley, Q. He, J. H. Harrhy, L. Lu, D. A. Crole, D. J. Morgan, E. N. Ntainjua, J. K. Edwards, A. F. Carley, A. Y. Borisevich, C. J. Kiely, G. J. Hutchings, *Science* **2016**, *351*, 965-968; b) G. M. Lari, B. Puértolas, M. Shahrokhi, N. López, J. Pérez-Ramírez, *Angew. Chem. Int. Ed.* **2017**, *56*, 1775-1779.

[6] a) M. Fukushima, K. Tatsumi, S. Tanaka, H. Nakamura, *Environ. Sci. Technol.* **1998**, *32*, 3948-3953; b) S. Kato, J. Jung, T. Suenobu, S. Fukuzumi, *Energy Environ. Sci.* **2013**, *6*, 3756-3764.

[7] a) K. Ohkubo, S. Fukuzumi, *Bull. Chem. Soc. Jpn.* **2009**, *82*, 303-315; b) K. Ohkubo, S. Fukuzumi, *Chem. Sci.* **2013**, *4*, 561-574; c) S. Fukuzumi, K. Ohkubo, *Org. Biomol. Chem.* **2014**, *12*, 6059-6071.

[8] a) A. J. Hoffman, E. R. Carraway, M. R. Hoffman, *Environ. Sci. Technol.* **1994**, *28*, 776-785; b) V. Maurino, C. Minero, G. Mariella, E. Pelizzetti, *Chem. Commun.* **2005**, 2627-2629; c) M. Teranishi, S. Naya, H. Tada, *J. Am. Chem. Soc.* **2010**, *132*, 7850-7851; d) W.-C. Hou, Y.-S. Wang, *ACS Sustainable Chem.* **2017**, *5*, 2994-3001; e) Y. Shiraishi, T. Takii, T. Hagi, S. Mori, Y. Kofuji, Y. Kitagawa, S. Tanaka, S. Ichikawa, T. Hirai, *Nat. Mater.* **2019**, *18*, 985-993.

[9] a) T. Honda, T. Kojima, S. Fukuzumi, *J. Am. Chem. Soc.* **2012**, *134*, 4196-4206; b) K. Mase, K. Ohkubo, S. Fukuzumi, *J. Am. Chem. Soc.* **2013**, *135*, 2800-2808.

[10] a) I. Hatay, B. Su, F. Li, M. A. Méndez, T. Khoury, C. P. Gros, J.-M. Barbe, M. Ersoz, Z. Samec, H. H. Girault, *J. Am. Chem. Soc.* **2009**, *131*, 13453-13459; b) B. Su, I. Hatay, A. Trojánek, Z. Samec, T. Khoury, C. P. Gros, J.-M. Barbe, A. Dania, P.-A. Carrupt, H. H. Girault, *J. Am. Chem. Soc.* **2010**, *132*, 2655-2662; c) P. Peljo, L. Murtomäki, T. Kallio, H.-J. Xu, M. Meyer, C. P. Gros, J.-M. Barbe, H. H. Girault, K. Laasonn, K. Kontturi, *J. Am. Chem. Soc.* **2012**, *134*, 5974-5984.

[11] C. J. Chang, Z.-H. Loh, C. Shi, F. C. Anson, D. G. Nocera, *J. Am. Chem. Soc.* **2004**, *126*, 10013-10020.

[12] a) G. Passard, A. M. Ullman, C. N. Brodsky, D. G. Nocera, *J. Am. Chem. Soc.* **2016**, *138*, 2925-2928; b) I. Monte-Pérez, S. Kundu, A. Chandra, K. E. Craigo, P. Chernev, U. Kuhlmann, H. Dau, P. Hildebrandt, C. Greco, C. V. Stappen, N. Lehnert, K. Ray, *J. Am. Chem. Soc.* **2017**, *139*, 15033-15042; c) Y.-H. Wang, M. L. Pegis, J. M. Mayer, S. S. Stahl, *J. Am. Chem. Soc.* **2017**, *139*, 16458-16461; d) Y.-H. Wang, Z. K. Goldsmith, P. E. Schneider, C. W. Anson, J. B. Gerken, S. Ghosh, S. Hammes-Schiffer, S. S. Stahl, *J. Am. Chem. Soc.* **2018**, *140*, 10890-10899; e) Y.-H. Wang, P. E. Schneider, Z. K. Goldsmith, S. Hammes-Schiffer, S. S. Stahl, *ACS Cent. Sci.* **2019**, *5*, 1024-1034.

[13] a) S. Fukuzumi, L. Tahsini, Y.-M. Lee. K. Ohkubo, W. Nam, K. D. Karlin, *J. Am. Chem. Soc.* **2012**, *134*, 7025-7035; b) D. Das, Y.-M. Lee, K. Ohkubo, W. Nam, K. D. Karlin, S. Fukuzumi, *J. Am. Chem. Soc.* **2013**, *135*, 2825-2834; c) M. A. Thorseth, C. E. Tornow, M. Tse, A. A. Gewirth, *Coord. Chem. Rev.* **2013**, *257*, 130-139; d) H. Kotani, T. Yagi, T. Ishizuka, T. Kojima, *Chem. Commun.* **2015**, *51*, 13385-13588.

[14] a) S. Liu. K. Mase, C. Bougher, S. D. Hicks, M. M. Abu-Omar, S. Fukuzumi, *Inorg. Chem.* **2014**, *53*, 7780-7788; b) J. Jung, S. Liu, K. Ohkubo, M. M. Abu-Omar, S. Fukuzumi, *Inorg. Chem.* **2015**, *54*, 4285-4291; c) S. L. Hooe, A. L. Rheingold, C. W. Machan, *J. Am. Chem. Soc.* **2018**, *140*, 3232-3241; d) S. L. Hooe, C. W. Machan, *J. Am. Chem. Soc.* **2019**, *141*, 4379-4387; e) L. Wang, M. Gennari, F. G. Cantú Reinhard, J. Gutiérrez, A. Morozan, C. Philouze, S. Demeshko, V. Artero, F. Meyer, S. P. de Visser, C. Duboc, *J. Am. Chem. Soc.* **2019**, *141*, 8244-8253.

[15] a) C. Kemal, T. C. Bruice, *Proc. Natl. Acad. Sci, USA* **1976**, *73*, 995-999; b) C. Kemal, T. W. Chan, T. C. Bruice, *J. Am. Chem. Soc.* **1977**, *99*, 7272-7286; c) T. C. Bruice, *Acc. Chem. Res.* **1980**, *13*, 256-262; d) S. Fukuzumi, T. Okamoto, *J. Chem. Soc. Chem. Commun.* **1994**, 521-522; e) S. Shibata, T. Suenobu, S. Fukuzumi, *Angew. Chem. Int. Ed.* **2013**, *53*, 12327-12331.

[16] K. Mase, K. Ohkubo, Z. Xue, H. Yamada, S. Fukuzumi, *Chem. Sci.* **2015**, *6*, 6496-6504.

[17] a) I. Hatay, B. Su, M. A. Méndez, C. Corminboeuf, T. Khoury, C. P. Gros, M. Bourdillon, M. Meyer, J.-M. Barbe, M. Ersoz, S. Zális, Z. Samec, H. H. Girault, *J. Am. Chem. Soc.* **2010**, *132*, 13733-13741; b) A. Trojánek, J. Langmaier, J. Šebera, S. Zális, J.-M. Barbe, H. H. Girault, Z. Samec, *Chem. Commun.* **2011**, *47*, 5446-5448; c) S. Wu, B. Su, *Chem. Eur. J.* **2012**, *18*, 3169-3173.

[18] a) K. Gong, F. Du, Z. Xia, M. Durstock, L. Dai, *Science* **2009**, *323*, 760-764; b) S. Wang, D. Yu, L. Dai, *J. Am. Chem. Soc.* **2011**, *133*, 5182-5185; c) Q. Li, B. W. Noffke, Y. Wang, B. Menezes, D. G. Peters, K. Raghavachari, L.-S. Li, *J. Am. Chem. Soc.* **2014**, *136*, 3358-3361; d) Y. Jiao, Y. Zheng, M. Jaroniec, S. Z. Qiao, *J. Am. Chem. Soc.* **2014**, *136*, 4394-4403.

[19] a) C. J. Medforth, M. O. Senge, K. M. Smith, L. D. Sparks, J. A. Shelnutt, *J. Am. Chem. Soc.* **1992**, *114*, 9859-9869; b) S. Fukuzumi, T. Honda, T. Kojima, *Coord. Chem. Rev.* **2012**, *256*, 2488-2502.

[20] a) S. Hiroto, Y. Miyake, H. Shinokubo, *Chem. Rev.* **2017**, *117*, 2910-3043; b) M. Roucan, K. J. Flanagan, J. O'Brien, M. O. Senge, *Eur. J. Org. Chem.* **2018**, 6432-6446.

[21] a) C. Liu, D.-M. Shen, Q.-Y. Chen, *J. Am. Chem. Soc.* **2007**, *129*, 5814-5815; b) B. K. Reddy, A. Basavarajappa, M. D. Ambhore, V. G. Anand, *Chem. Rev.* **2017**, *117*, 3420-3443; c) Y. Wu, N. Rodrigues-López, D. Villagrán, *Chem. Sci.* **2018**, *9*, 4689-4695.

[22] W. Suzuki, H. Kotani, T. Ishizuka, Y. Shiota, K. Yoshizawa, T. Kojima, *Angew. Chem. Int. Ed.* **2018**, *57*, 1973-1977.

[23] a) M. Pohl, H. Schmickler, J. Lex,E. Vogel, *Angew. Chem. Int. Ed.* **1991**, *30*, 1693-1697; b) J. Setsune, K. Kashihara, K. Wada, H. Shinozaki, *Chem. Lett.* **1999**, 847-848; c) A. M. Bruce, E. S. Weyburne, J. T. Engle, C. J. Ziegler, G. R. Geirer, III, *J. Org. Chem.* **2014**, *79*, 5664-5672; d) B. H. Solis, A. G. Macher, D. K. Dogutan, D. G. Nocera, S. Hammes-Schiffer, *Proc. Natl. Acad. Sci. USA* **2016**, *113*, 485-492.

[24] a) T. Kojima, K. Hanabusa, K. Ohkubo, M. Shiro, S. Fukuzumi, *Chem. Commun.* **2008**, 6513-6515; b) S. Ishihara, J. P. Hill, A. Shundo, G. J. Richards, J. Labuta, K. Ohkubo, S. Fukuzumi, A. Sato, M. R. J. Elsegood, S. J. Teat, K. Ariga, *J. Am. Chem. Soc.* **2011**, *133*, 16119-16126.

[25] a) M. Kielmann, M. O. Senge, *Angew. Chem. Int. Ed.* **2019**, *58*, 418-441; b) K. Norvaiša, K. Flanagan, D. Gibbons, M. O. Senge, *Angew. Chem. Int. Ed.* **2019**, *58*, 16553-16557.

[26] W. Suzuki, H. Kotani, T. Ishizuka, T. Kojima, *J. Am. Chem. Soc.* **2019**, *141*, 5987-5994.

[27] S. Fukuzumi, S. Kuroda, T. Tanaka, *J. Am. Chem. Soc.* **1985**, *107*, 3020-3027.

[28] T. Kojima, T. Nakanishi, R. Harada, K. Ohkubo, S. Yamauchi, S. Fukuzumi, *Chem. Eur. J.* **2007**, *13*, 8714-8725.

[29] W. Suzuki, H. Kotani, T. Ishizuka, K. Ohkubo, Y. Shiota. K. Yoshizawa, S. Fukuzumi, T. Kojima, *Chem.-Eur. J.* **2017**, *23*, 4669-4679.

[30] K. Izutsu, Acid–Base Dissociation Constants in Dipolar Aprotic Solvents, Blackwell Scientific Publications, Oxford, 1990.

[31] Y. Fang, Y. G. Gorbunova, P. Chen, X. Jiang, M. Manowong, A. A. Sinelshchikova, Y. Y. Enakieva, A. G. Martynov, A. Y. Tsivadze, A. Bessmertnykh-Lemeune, C. Stern, R. Guillard, K. M. Kadish, *Inorg. Chem.* **2015**, *54*, 3501-3512.

[32] E. Aoki, W. Suzuki. H. Kotani, T. Ishizuka, H. Sakai, T. Hasobe, T. Kojima, *Chem. Commun.* **2019**, *55*, 4925-4928.

Entry for the Table of Contents (Please choose one layout)

Layout 1:

FULL PAPER

Selective two-electron reduction of dioxygen to hydrogen peroxide has been achieved using two *N*,*N*'-dimethylated porphyrin isomers as catalysts. Based on kinetic analysis, we have revealed the difference of position on pyrrolic protons in reduced porphyrinoids causes difference in reaction mechanisms of dioxygen reduction with regard to the proton source of H_2O_2, whether pyrrole N-H protons or external protons.

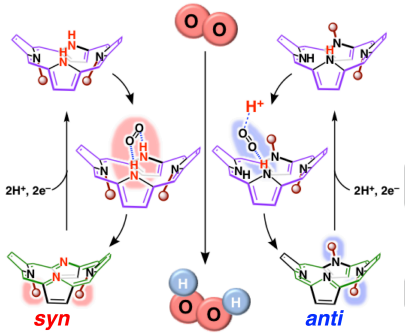

Wataru Suzuki, Hiroaki Kotani, Tomoya Ishizuka, and Takahiko Kojima*

Page No. – Page No.

A Mechanistic Dichotomy in Two-Electron Reduction of Dioxygen Catalyzed by *N*,*N*'-Dimethylated Porphyrin Isomers